Localized spin modes in ferromagnetic cylindrical dots with in-plane magnetization

2007 J. Phys.: Condens. Matter 19 305012

(http://iopscience.iop.org/0953-8984/19/30/305012)

IOP PUBLISHING JOURNAL OF PHYSICS: CONDENSED MATTER

J. Phys.: Condens. Matter **19** (2007) 305012 (15pp) doi:10.1088/0953-8984/19/30/305012

Localized spin modes in ferromagnetic cylindrical dots with in-plane magnetization

Roberto Zivieri[1], **Giorgio Santoro**[2] **and Anna Franchini**[2]

[1] CNISM, Unità di Ferrara and Dipartimento di Fisica, Università di Ferrara, Via Saragat 1, I-44100 Ferrara, Italy
[2] CNISM, Unità di Modena and Dipartimento di Fisica, Università di Modena and Reggio Emilia, Via Campi 213/A, I-41100 Modena, Italy

E-mail: zivieri@fe.infn.it

Received 5 February 2007, in final form 22 March 2007
Published 13 July 2007
Online at stacks.iop.org/JPhysCM/19/305012

Abstract

A study of spin localized excitations in ferromagnetic tangentially magnetized dots of cylindrical shape and of nanometric size is presented. A recently formulated variational theory permits us to study the most representative localized spin modes of the spectrum. One of these, the fundamental mode, is mainly localized in the central part of the dot endfaces and is analogous to the Kittel uniform mode in ellipsoids. We also investigate the dynamical properties of spin modes localized in the lateral part of the dot endfaces along the direction of the applied magnetic field, studying the dependence of their localization on the variational parameter and the applied magnetic field. Finally, a comparison of the calculated frequencies of some of these localized modes with available experimental data is performed.

1. Introduction

In this last decade the study of the dynamical properties of magnetic nanostructures has been of great interest both experimentally and from a theoretical point of view. A great deal of experimental work has shown evidence for discretization effects due to the lateral confinement of nanostructured materials of different shapes [1, 2]. In order to explain the measurements, great advances in the calculation of magnetic normal modes have been made in recent years.

One can distinguish between analytical and micromagnetic calculations performed to describe the dynamical properties of confined magnetic systems. To understand the dynamical properties of discs, two analytical models that describe some of the spin excitations in tangentially magnetized discs with strong approximations on the boundary conditions and on the choice of eigenfunctions have recently been formulated [3, 4]. Micromagnetic calculations based on a dynamical matrix approach applied to cylindrical dots [5] have shed light on

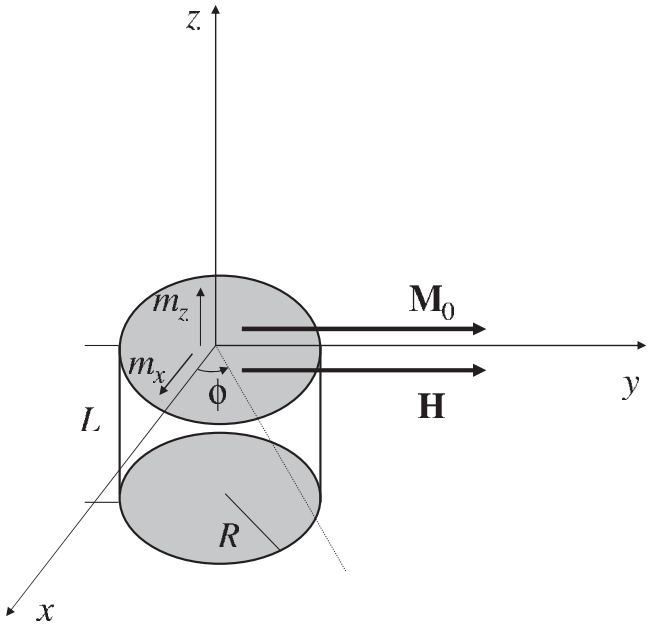

Figure 1. Geometry of the system and the reference frame.

the most important properties of spin modes determining the mode profiles and the mode eigenfrequencies. On the other hand, a very recent theory of spin modes able to encompass the dynamical properties of spin modes in cylindrical dots, which proposes suitable trial eigenfunctions for each family of modes and obtains new boundary conditions, has been developed by Zivieri and Stamps [6].

In the present paper we show some interesting applications of this theory for the study of the dynamical properties of the most important localized spin modes of the spectrum in a cylindrical dot with a radius in the nanometric range and for different aspect ratios. Firstly, a detailed study of the dynamical properties of the most representative mode, the fundamental (F), which is mainly localized in the central part of the dot endfaces is carried out. Moreover, the most representative spin modes localized in the region close to the dot edges (end modes) are investigated and the dependence of their localization on the variational parameter is examined. The outline of this paper is as follows. In section 2 we recall the formalism of the variational theory formulated in [6]. Section 3 is devoted to an investigation of the dynamical properties of the F mode that represents the resonant mode of the spectrum. In section 4 we present the application of the variational method to end modes, studying the lateral localization in detail. The comparison of the calculated frequencies of the most representative localized modes with available Brillouin light scattering (BLS) experimental data is performed in section 5. Conclusions are drawn in the final section 6.

2. Theory

We choose a Cartesian reference frame (x, y, z) with the z-axis normal to the dot endfaces and the static magnetization $\mathbf{M}_0$ aligned along the y-axis and assumed uniform (see figure 1). Let us recall the basic equations of the theoretical model formulated in [6]. The physical quantities

are expressed in a cylindrical coordinate system (ρ, ϕ, z). The total magnetization given by the sum of a static and a small dynamic part, respectively, is $\mathbf{M}(\boldsymbol{\rho}, t) = \mathbf{M}_0 + \mathbf{m}(\boldsymbol{\rho}, t)$. In the model the dynamic magnetization of the spin modes was supposed uniform along the z-direction. As already pointed out in [6], this assumption seems less realistic for dots of aspect ratio $\beta > 0.25$ with $\beta = L/R$ (L is the dot thickness and R is the dot radius). Neglecting second-order dynamic terms, the linearized equations of motion are

$$-\frac{1}{\gamma}\frac{\partial \mathbf{m}(\boldsymbol{\rho}, t)}{\partial t} = \mathbf{m}(\boldsymbol{\rho}, t) \times \mathbf{H}^{\mathrm{eff}}(\boldsymbol{\rho}) + \mathbf{M}_0 \times \mathbf{h}_{\mathrm{d}}^{\mathrm{eff}}(\boldsymbol{\rho}, t) \tag{1}$$

where γ is the gyromagnetic ratio. The static internal field to first-order [7] may be written as $\mathbf{H}^{\mathrm{eff}}(\boldsymbol{\rho}) = \mathbf{H} + \mathbf{H}_{\mathrm{s}}^{(1)}(\boldsymbol{\rho})$. $\mathbf{H}$ is the external magnetic field, $\mathbf{H}_{\mathrm{s}}^{(1)}(\boldsymbol{\rho})$ is the first-order static demagnetizing field $\mathbf{H}_{\mathrm{s}}^{1}(\mathbf{r})$ averaged over z and z' and the dynamic effective field is given by $\mathbf{h}_{\mathrm{d}}^{\mathrm{eff}}(\boldsymbol{\rho}, t) = \mathbf{h}_{\mathrm{exch}}(\boldsymbol{\rho}, t) + \mathbf{h}_{\mathrm{d}}(\boldsymbol{\rho}, t)$. $\mathbf{h}_{\mathrm{exch}}(\boldsymbol{\rho}, t) = \alpha\nabla^2\mathbf{m}(\boldsymbol{\rho}, t)$ is the dynamic nonuniform exchange field where $\alpha = \frac{2A}{M_{\mathrm{s}}^2}$ is the exchange constant and A is the exchange stiffness constant. $\mathbf{h}_{\mathrm{d}}(\boldsymbol{\rho}, t)$ is the dynamic dipolar field expressed as a functional of the dynamic magnetization. The eigenfunctions are the dynamic magnetization components $m_x(\boldsymbol{\rho}, t)$ and $m_z(\boldsymbol{\rho}, t)$. Their amplitudes m_{0x} and m_{0z} define the precession plane and are assumed to vary in time according to $\exp(-\mathrm{i}\omega t)$ with ω the spin mode frequency. Simplifying the temporal dependence and writing (1) in terms of components we get after straightforward algebra

$$\Omega^2 = \left[\frac{\int \mathrm{d}^2\boldsymbol{\rho} m_x^{*n'}(\boldsymbol{\rho})(H + H_{\mathrm{s}}^{y}(\boldsymbol{\rho}) - \alpha M_{\mathrm{s}}\nabla^2)m_x^{n}(\boldsymbol{\rho}) - M_{\mathrm{s}}\int \mathrm{d}^2\boldsymbol{\rho} m_x^{*n'}(\boldsymbol{\rho})h_x^{n}(\boldsymbol{\rho})}{\int \mathrm{d}^2\boldsymbol{\rho} m_x^{*n'}(\boldsymbol{\rho})m_x^{n}(\boldsymbol{\rho})}\right] \times \left[\frac{\int \mathrm{d}^2\boldsymbol{\rho} m_z^{*n'}(\boldsymbol{\rho})(H + H_{\mathrm{s}}^{y}(\boldsymbol{\rho}) - \alpha M_{\mathrm{s}}\nabla^2)m_z^{n}(\boldsymbol{\rho}) - M_{\mathrm{s}}\int \mathrm{d}^2\boldsymbol{\rho} m_z^{*n'}(\boldsymbol{\rho})h_z^{n}(\boldsymbol{\rho})}{\int \mathrm{d}^2\boldsymbol{\rho} m_z^{*n'}(\boldsymbol{\rho})m_z^{n}(\boldsymbol{\rho})}\right] \tag{2}$$

where $\Omega = \omega/\gamma$. $H_{\mathrm{s}}^{y}(\boldsymbol{\rho}) = -4\pi M_{\mathrm{s}} N_{yy}(\boldsymbol{\rho})$ is the y-component of the first-order demagnetizing field averaged over z and z'. $N_{yy}(\boldsymbol{\rho})$, the static demagnetizing tensor component along the y-direction, plays the role of the static demagnetizing factor along y; $M_{\mathrm{s}} = |\mathbf{M}_0|$ is the saturation magnetization.

Let us recall the integrals appearing in (2) which will be useful for the next discussion.

(i) Normalization integral
$N_i^{nn'} = \int \mathrm{d}^2\boldsymbol{\rho} m_i^{n'}(\boldsymbol{\rho}) m_i^{n}(\boldsymbol{\rho}) = N_i^{n}\delta_{nn'}$

(ii) Exchange integral
$E_i^{nn'} = \bar{E}_i^{nn'}/N_i^{nn'}$ with $\bar{E}_i^{nn'} = -\alpha M_{\mathrm{s}}\int \mathrm{d}^2\boldsymbol{\rho} m_i^{*n'}(\boldsymbol{\rho})\nabla^2 m_i^{n}(\boldsymbol{\rho}) = \bar{E}_i^{n}\delta_{nn'}$ defined including the minus sign.

(iii) Static demagnetizing integral
$D_i^{nn'} = \bar{D}_i^{nn'}/N_i^{nn'}$ with $\bar{D}_i^{nn'} = \int \mathrm{d}^2\boldsymbol{\rho} m_i^{*n'}(\boldsymbol{\rho}) H_{\mathrm{s}}^{y}(\boldsymbol{\rho}) m_i^{n}(\boldsymbol{\rho}) = \bar{D}_i^{n}\delta_{nn'}$

(iv) Dynamic demagnetizing integral
$d_i^{nn'} = \bar{d}_i^{nn'}/N_i^{nn'}$ with $\bar{d}_i^{nn'} = M_{\mathrm{s}}\int \mathrm{d}^2\boldsymbol{\rho} m_i^{*n'}(\boldsymbol{\rho}) h_{\mathrm{d}i}^{n}(\boldsymbol{\rho}) = \bar{d}_i^{n}\delta_{nn'}$ $(i = x, z)$ defined here including M_{s}.

The eigenvalues are calculated in the diagonal approximation, i.e. for $n = n'$ with n labelling the quantization number that gives the number of nodes throughout the dot. By means of this approximation we do not take into account the dipole–dipole interaction of spin wave modes of different types ($n \neq n'$) as also shown in the definition of the demagnetizing integrals listed in (iii) and (iv). This interaction is caused by the non-diagonal elements of both the static and dynamic demagnetizing integrals that have been neglected in the derivation of equation (2). We emphasize that in (2) we consider only an implicit dependence on the azimuthal index m,

because the spin mode trial eigenfunctions $m_i^n(\boldsymbol{\rho})$ are written as Bessel expansions of increasing order of stationary waves truncated at the second-order. Finally, results of the variational theory are applicable to arrays where the interdot distance is larger than or equal to the dot diameter $2R$ and is also larger than the dot thickness L. In this way the interdot coupling may be neglected and it is possible to study the dynamical properties of a single cylindrical dot.

3. Fundamental mode

In this section we discuss the localization of the most representative mode, called the fundamental (F), whose profile is mainly localized in the central part of the dot endfaces especially along the direction of the static magnetization. We give a quantitative derivation of the approximated Kittel equation proposed in [6] to describe the dynamics of the F mode in cylindrical dots whose radii are in the nanometric range. This excitation is analogous to the Kittel uniform mode in ellipsoids [8]. In particular, for the case of tangentially thin magnetized cylindrical dots, the large value of the static demagnetizing factor on the dot border along $\mathbf{M}_0$ (the y-direction) is responsible for the strong lateral pinning of the F mode along this direction. On the other hand, the profile of the F mode is almost flat in the remaining part of the dot endfaces, especially along the x-direction where the demagnetizing factor has a very reduced spatial variation. Hence, it is plausible to assume in the first place a mode characterized by a vanishing quantized wavenumber attributing its reduced amplitude close to the boundary to the surface pinning, to the nonuniformity of the static demagnetizing field and also to the rotation of the static magnetization with respect to the direction of the applied field towards the dot edge. Due to this assumption the exchange integral of (2), proportional to the square of the quantized wavenumber, vanishes. Furthermore, the static demagnetizing integral turns out to be proportional to the static demagnetizing tensor component along the y-direction averaged over the dot area given by $N_{yy} = \langle N_{yy}(\boldsymbol{\rho})\rangle$ where $\langle\cdots\rangle$ denotes the geometric average. Similarly, the dynamic dipolar integrals d_x and d_z reduce to quantities proportional to the static demagnetizing tensor components along the x- and z-directions averaged over the dot area given by $N_{xx} = \langle N_{xx}(\boldsymbol{\rho})\rangle$ and $N_{zz} = \langle N_{zz}(\boldsymbol{\rho})\rangle$, respectively; moreover, $N_{xx} = N_{yy}$ for a circular cylinder. Therefore, from (2) written in the diagonal approximation for the case $n = n' = 0$ and from the Brown theorem ($N_{zz} = 1 - 2N_{yy}$) [9] we get the Kittel equation for the resonance mode in cylindrical dots: $\Omega^2 = [H \times (H + 4\pi M_s(1 - 3N_{yy}))]$. In particular, $N_{yy} = N_{\parallel}$ where $N_{\parallel}$ is the effective in-plane demagnetizing factor obtained by means of the average over the dot area.

Let us obtain the approximated formula. We consider the region $0 \leqslant \rho \leqslant R/2$. This choice is motivated by the peculiar spatial dependence along the y-direction of the demagnetizing factor which drastically changes slope at about $\rho = R/2$. As a matter of fact, in this region the value of $N_{yy}(\boldsymbol{\rho})$ increases by about only 27% along the y-direction with respect to the value in the dot centre $N_{yy}(\rho = 0)$. Instead, for $R/2 \leqslant \rho \leqslant R$ it rapidly increases, assuming at $\rho = R$ a value about three times larger than the one assumed at $\rho = R/2$. The high nonuniformity gradually reduces going towards the x-direction, where it does not vary appreciably. It is important to note that this is a general trend independent from the dot aspect ratio considered. Correspondingly, the F mode amplitude reduces by only 27% in the region $0 \leqslant \rho \leqslant R/2$ along the y-direction. This amplitude reduction becomes less important going towards the x-direction where the profile is almost flat. Instead, in the region $R/2 \leqslant \rho \leqslant R$ the amplitude of the F mode, especially along the y-direction, almost vanishes, because of the rotation of the static magnetization and of the strong nonuniformity of the demagnetizing field together with the strong pinning on the border. This behaviour, together with the very similar behaviour of the demagnetizing factor, allows us to take as realistic the

average of $N_{yy}(\boldsymbol{\rho})$ over a dot of radius $\bar{R} = R/2$ which corresponds more or less to the point where important changes of slope of $N_{yy}(\boldsymbol{\rho})$ and of the F mode profile along the y-direction occur. The demagnetizing tensor component along the y-direction obtained in [6] reads $N_{yy}(\rho, \phi) = R[\int_0^\infty \mathrm{d}k\,\chi(kL)J_1(kR)J_0(k\rho)\sin^2\phi + \int_0^\infty \mathrm{d}k\,\chi(kL)J_1(kR)J_1(k\rho)/(k\rho)\cos 2\phi]$ and its average over the dot area of radius $\bar{R} = R/2$ is

$$\bar{N}_{yy} = 2\int_0^\infty \mathrm{d}t\,\frac{1}{t}\chi(\beta t)J_1(t/2)J_1(t) \tag{3}$$

where $t = kR$ with k the wavevector of the Green's function Fourier representation used for the calculation of $N_{yy}(\boldsymbol{\rho})$; the dynamical inverse susceptibility $\chi(\beta t) = 1 - \frac{1-\mathrm{e}^{-\beta t}}{\beta t}$ is the result of the average over z and z'. At this stage we may insert into the Kittel equation for cylindrical dots the demagnetizing tensor component $\bar{N}_{yy}$ calculated according to (3) in place of N_{yy}. Nevertheless, from the calculation of the demagnetizing tensor component in the centre given by $N_{yy}(\rho = 0) = \frac{\beta}{2(\sqrt{1+\beta^2}+1)}$, we have found that this value represents a very good approximation of $\bar{N}_{yy}$ in the range of aspect ratios of interest, i.e. for $\beta < 1$. In particular, the calculated $N_{yy}(\rho = 0)$ almost overlaps with $\bar{N}_{yy}$, underestimating it by less than 10% for the aspect ratios β considered and yielding a slight overestimation in the corresponding calculated F mode frequency. Therefore, we may in turn substitute $N_{yy}(\rho = 0)$ in place of $\bar{N}_{yy}$ into the Kittel equation getting

$$\tilde{\Omega}^2 = [H \times [H + 4\pi M_s(1 - 3N_{yy}(\rho = 0))]] \tag{4}$$

which represents our approximated Kittel formula for the calculation of the F mode frequency proposed in [6].

Furthermore, for $\beta \ll 1$ ('ultrathin' dot limit) a realistic evaluation of the F mode frequency may also be obtained by means of the Kittel equation for cylindrical dots with the effective in-plane demagnetizing factor $N_\parallel$ in place of $N_{yy}(\rho = 0)$. Even though $N_\parallel$ is slightly larger than $N_{yy}(\rho = 0)$ the frequency evaluated with $N_\parallel$ is very close to the one determined using $N_{yy}(\rho = 0)$ in the 'ultrathin' dot limit.

The F mode profiles of the m_x component along both the y-direction and the x-direction for a dot with $R = 100$ nm and $L = 50$ nm are shown in figures 2(a) and (c), respectively; the corresponding spatial variations of $N_{yy}(\rho, \phi)$ are shown in figures 2(b) and (d), respectively. In figure 2(a) one sees that the F mode is localized in the central area of the dot endface and that its amplitude almost vanishes on the dot border, especially because of the nonuniform demagnetizing field and of the strong surface pinning along the y-direction; as shown in figure 2(c) instead its profile does not vary appreciably along the x-direction. An analogous behaviour is also shown by the $N_{yy}(\rho, \phi)$ demagnetizing factor. The F mode profile depicted in figure 2 is the result of the Bessel series expansion of a symmetric (S) stationary wave of backward-like (BA) nature truncated at the second-order [6], i.e. $m_i = m_{0i}[J_0(k_0\rho) + 2J_2(k_0\rho)\cos 2\phi]$ with J_0 and J_2 being Bessel functions of the first kind of zero- and second-order, respectively; the complex dynamic magnetization amplitudes m_{0i} are assumed proportional ($i = x, z$) and k_0 is the quantized wavenumber. This functional form is taken under the assumption that the F mode is the first BA mode with no nodes throughout the dot [5], but note that it could also be classified as the first Damon–Eshbach-like (DE) mode with no nodes. Even though within this framework the F mode does not have an effective quantized wavenumber determined by means of the boundary condition the lateral pinning causes a reduction of its amplitude, especially along the y-direction, giving rise likewise to a non-vanishing quantized wavenumber. In order to reproduce the strong pinning at the boundary we have taken $k_0 = 1.5 \times 10^5$ cm^{-1}. On the other hand, it is important to note that a numerical value slightly larger than k_0 could be also approximately obtained as

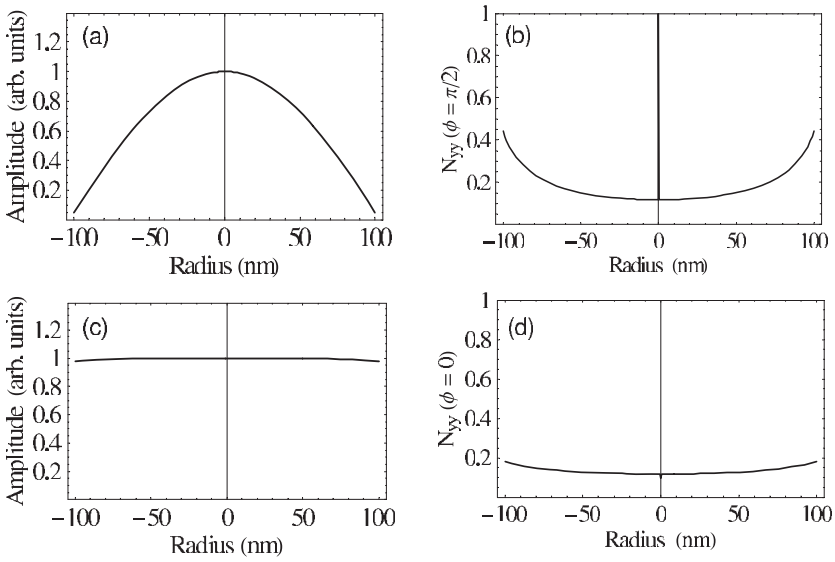

Figure 2. (a) Spatial profile of the F mode along the y-direction. The corresponding quantized wavenumber is $k_0 = 1.5 \times 10^5$ cm^{-1}. (b) $N_{yy}(\rho, \phi)$ along the the y-direction ($\phi = \pi/2$). (c) Spatial profile of the F mode along the x-direction. (d) $N_{yy}(\rho, \phi)$ along the the x-direction ($\phi = 0$).

the first non-vanishing solution k_2 of the S BA mode boundary condition (cf equation (44) in [6]). If one assumes that the $n = 2$ mode, classified as a 2-BA by Zivieri and Stamps [6] with $m_i = m_{0i}[J_0(k_2\rho) + 2J_2(k_2\rho)\cos 2\phi]$, is affected by the demagnetizing factor in the dot centre ($N_{yy}(\rho = 0)$) this mode could be considered the F mode of the spectrum, because the two nodes very close to the dot border along the y-direction may be attributed to the lateral pinning effect. Taking account of the above assumption, the frequency of this mode could thus be calculated according to equation (4). In this way, the F mode description would be very similar to the one given for the F mode in the vortex state whose quantized wavenumber was obtained as the first non-vanishing solution of the radial boundary condition [10]. A non-vanishing quantized wavenumber gives rise to both exchange and dipolar dynamic fields that would add a contribution to the F mode frequency, but a numerical evaluation performed for different aspect ratios has confirmed that these fields may be considered negligible. Hence, the F mode dynamics in the saturated state may be actually described solely in terms of static dipolar energy. Finally, it is also reasonable to consider the F mode profile in the saturated state to also be substantially uniform along the dot thickness for dots of moderate aspect ratio, as also suggested by micromagnetic calculations.

4. End modes

An interesting family of spin excitations, recently observed and described in stripes [11] and in dots of different shapes [4, 5, 12], is represented by the so-called end modes that are spin excitations localized in the lateral part of the dot endfaces along the direction of the applied field (y-direction). Their localization is mainly due to the strongly inhomogeneous internal field in the lateral region of the dot endfaces along the y-direction.

Since in [6] the trial eigenfunctions of end modes were proposed without giving their detailed derivation, we believe that it is now useful to present their derivation for both

symmetric (S) and antisymmetric (AS) end modes (see the following discussion for the definition of symmetry). It is plausible to derive the eigenfunctions from the truncated Bessel series expansion of BA modes assuming that the corresponding quantized wavenumber becomes complex. The real part of the quantized wavenumber characterizes the dynamics of end modes giving the possibility that nodal surfaces parallel to the x-axis and close to the dot edges could also be present, as found for example in dots of elliptical shape by means of micromagnetic calculations [12]. Instead, the imaginary part modulates the spatial profiles of end modes describing their lateral localization. This treatment is classical like the approach proposed in [11] where the analogue of the quasi-classical quantization condition in a potential well was applied in the lateral region of the stripe. Within that approach the mode was described by means of a real quantized wavenumber dependent on the spatial coordinate in the lateral region of the dot where the internal field is highly inhomogeneous. The mode could thus not exist within the central region of the dot characterized by the potential barrier represented by the internal field. Instead, in the present model the generic end mode is characterized by an amplitude depending on the spatial coordinate in the whole dot. The strong amplitude attenuation in the central part of the dot, which is indirectly related to the imaginary part of the quantized wavenumber, thus plays the role of the effect of the potential barrier on the mode amplitude. On the other hand, taking into account that the linearized equation of motion is a Schrödinger-like equation one could study the system following a further approach. As a matter of fact, one could find, analogously to the one-dimensional solution of the Schrödinger equation in quantum mechanics, the one-dimensional (y-direction) solution of the Schrödinger-like equation in this system. One should thus separate the dot endfaces into three regions characterized by the two lateral potential wells and by the central potential barrier studying the spin dynamics not only in the lateral regions but also in the central region. The quantized wavenumber dependent from the spatial coordinate would be real in the lateral regions and, due to the penetration inside the potential barrier, it would be purely imaginary in the central region. Nevertheless, we will not follow this approach here.

As outlined in [6], the equation of motion would admit an eigenfunction with a complex wavevector if in principle a phenomenological damping term is included in the effective field. This term should vanish for the other families of modes studied in [6] whose amplitudes are not affected by the potential barrier. It is well-known from the solution of the linearized Landau–Lifshitz–Gilbert equation for ferromagnetic films that the Gilbert term is responsible for the complex frequency of spin waves and the temporal damping in the presence of a real wavevector. Similarly, it may be possible in general to add a Gilbert-type term to the dynamic effective field appearing in the linearized equation of motion relating it to the spatial damping of the mode in the material. It is not our purpose to deal with this term here, but note that it should be taken into account to explain the presence of a complex wavevector in the presence of a real frequency. In particular, for a confined system like a dot whose dynamical properties are described by (1) and by boundary conditions a complex quantized wavenumber $k_n^{\mathrm{C}} = k_n^{\mathrm{R}} \pm \mathrm{i}k_n^{\mathrm{I}}$ would arise with the inclusion of the spatial damping term into the dynamic effective field $\mathbf{h}_{\mathrm{d}}^{\mathrm{eff}}(\boldsymbol{\rho}, t)$ of (1) in the presence of a real frequency. k_n^{R} is the real part of the quantized wavenumber, k_n^{I} is the imaginary part of the quantized wavenumber and n is the quantization number. In order to obtain a complex quantized wavenumber in the presence of a real frequency it is sufficient to substitute a trial eigenfunction in the form of a stationary wave in (1) provided that the damping term is included into the dynamic effective field of (1). Then, one finds the complex quantized wavenumber as a function of the assumed known real frequency by means of the inversion of the dispersion relation. The factor related to k_n^{I} and given by $\cosh(k_n^{\mathrm{I}}\rho \sin\phi)$ for both S and AS end mode eigenfunctions (see the following discussion) plays the role of the amplitude attenuation of the laterally localized spin mode.

This behaviour may be considered analogous to that of electromagnetic waves in dielectrics and in magnetic media where plane waves, the solution of the Maxwell equations, are characterized by a complex wavevector. We recall that the analogy of the dynamical properties of end modes with electromagnetic waves in homogeneous media is only formal. Actually, the assumed complex quantized wavenumber of end modes is only a tool to describe in a phenomenological way the localization of end modes at the dot edges, while the complex wavevector of electromagnetic waves in homogeneous media is really related to the optical properties of the material, like for example its complex index of refraction. Nevertheless, bearing in mind this difference the analogy may be further extended taking into account the fact that the dynamical properties of end modes are similar to those of BA modes. Actually, within this model where eigenfunctions are taken as Bessel expansions of resonance modes truncated at the second-order, the end modes are quasi-transverse excitations with a complex quantized wavenumber. The magnetization amplitude components m_{0x} and m_{0z} are along the x and z axes, respectively and the quantized wavenumber is prevalently along the y-direction. Hence, the behaviour is very similar to that of electromagnetic waves except for the fact that in this latter case the condition of transversality is rigorously fulfilled. As a matter of fact, if we suppose that the electric field is parallel to the z-axis and the magnetic field is parallel to the x-axis the wave propagation is parallel to the y-axis. Consequently, the x-component of the dynamic magnetization amplitude m_{0x} would play the role of the magnetic field amplitude and the z-component of the dynamic magnetization amplitude m_{0z} would play the role of the electric field amplitude. Moreover, the electromagnetic wavevector parallel to the y-axis should be substituted by the end mode quantized wavenumber which is prevalently along the y-direction.

Within the variational method we write $k_n^{\mathrm{C}} = k_n^{\mathrm{R}} \pm \mathrm{i}\epsilon k_n^{\mathrm{I}}$ where ϵ is the variational parameter. The $\pm$ sign in front of k_n^{I} is due to the fact that we choose $\epsilon > 0$, but note that it is $\Omega(-\epsilon) = \Omega(\epsilon)$ for each ϵ. A S resonant mode prevalently oscillating along the y-direction, namely $k_x^n \simeq 0$ may be represented by a cosine function $\cos(k_n^{\mathrm{C}}\rho\sin\phi)$ where $y = \rho\sin\phi$ and the subscript labelling the y-direction of the quantized wavenumber has been omitted. Substituting into the argument of the cosine function $k_n^{\mathrm{C}} = k_n^{\mathrm{R}} \pm \mathrm{i}\epsilon k_n^{\mathrm{I}}$ and keeping only the real part of the trigonometric expansion we get for the dynamic magnetization $m_i^n(\rho,\phi) = m_0^i[\cos(k_n^{\mathrm{R}}\rho\sin\phi)\cosh(\epsilon k_n^{\mathrm{I}}\rho\sin\phi)]$ where $\cosh(\epsilon k_n^{\mathrm{I}}\rho\sin\phi) = \cos(\epsilon \mathrm{i}k_n^{\mathrm{I}}\rho\sin\phi)$. Moreover, because of this assumption also the dynamic magnetization amplitudes m_0^i, which are in general complex, become real. The S mode expansion in terms of Bessel functions of the first kind (cf equation (31) of [6]) inside a cylinder truncated at the second-order leads to

$$m_i^n(\rho,\phi) = m_{0i}[J_0(k_n^{\mathrm{R}}\rho) + 2J_2(k_n^{\mathrm{R}}\rho)\cos 2\phi][I_0(\epsilon k_n^{\mathrm{I}}\rho) - 2I_2(\epsilon k_n^{\mathrm{I}}\rho)\cos 2\phi] \tag{5}$$

where $I_0(\epsilon k_n^{\mathrm{I}}\rho)$ and $I_2(\epsilon k_n^{\mathrm{I}}\rho)$ are the modified Bessel functions of the first kind of zero- and of second-order, respectively, with $I_0(\epsilon k_n^{\mathrm{I}}\rho) = J_0(\epsilon \mathrm{i}k_n^{\mathrm{I}}\rho)$, $I_2(\epsilon k_n^{\mathrm{I}}\rho) = -J_2(\epsilon \mathrm{i}k_n^{\mathrm{I}}\rho)$, $I_0(\epsilon k_n^{\mathrm{I}}\rho) = I_0(-\epsilon k_n^{\mathrm{I}}\rho)$ and $I_2(\epsilon k_n^{\mathrm{I}}\rho) = I_2(-\epsilon k_n^{\mathrm{I}}\rho)$.

Similarly, the trial eigenfunctions of the AS end modes may also be easily obtained. An AS resonant mode which prevalently oscillates along the y-direction, namely $k_x^n \simeq 0$, may be represented by a sine function $\sin(k_n^{\mathrm{C}}\rho\sin\phi)$ where the meaning of the symbols is the same as for the S modes. Substituting the complex quantized wavenumber $k_n^{\mathrm{C}} = k_n^{\mathrm{R}} \pm \mathrm{i}\epsilon k_n^{\mathrm{I}}$ into the argument of the sine function and keeping only the real part of the trigonometric expansion we get for the dynamic magnetization components the expression $m_i^n(\rho,\phi) = m_0^i[\sin(k_n^{\mathrm{R}}\rho\sin\phi)\cosh(\epsilon k_n^{\mathrm{I}}\rho\sin\phi)]$. Also in this case the dynamic magnetization amplitudes turn out to be real. Again, using the Bessel expansion for AS modes (cf equation (32) of [6]) truncated at the second-order we obtain

$$m_i^n(\rho,\phi) = m_{0i}[2J_1(k_n^{\mathrm{R}}\rho)\sin\phi + 2J_3(k_n^{\mathrm{R}}\rho)\sin 3\phi][I_0(\epsilon k_n^{\mathrm{I}}\rho) - 2I_2(\epsilon k_n^{\mathrm{I}}\rho)\cos 2\phi]. \tag{6}$$

In (5) and in (6) we make the initial assumption on the complex quantized wavenumber k_n^{C} given by $k_n^{\mathrm{R}} = k_n^{\mathrm{I}}$. The first and the most representative of S end modes, the end mode (EM) together with the corresponding AS EM will be described later in this section. Note that the EM (AS EM) is a laterally localized mode along the direction of the applied magnetic field symmetric (antisymmetric) with respect to a plane normal to the dot endfaces passing through the x-axis. These modes do not have nodal surfaces along both x- and y-directions.

Finally, from (5) and (6) and from the expansion of S and AS resonance modes (cf equations (31) and (32) of [6], respectively) we may also give the trial eigenfunctions of modes which mix features of S end modes or AS end modes with those of DE modes. This family of modes has also been found by means of micromagnetic calculations performed in dots of different shapes [5, 12]. Their corresponding eigenfunctions may be represented in the form

$$m_i^{n\bar{n}}(\rho,\phi) = m_{0i}[J_0(k_n^{\mathrm{R}}\rho) + 2J_2(k_n^{\mathrm{R}}\rho)\cos 2\phi][I_0(\epsilon k_n^{\mathrm{I}}\rho) - 2I_2(\epsilon k_n^{\mathrm{I}}\rho)\cos 2\phi] \times [J_0(k'_{\bar{n}}\rho) - 2J_2(k'_{\bar{n}}\rho)\cos 2\phi] \tag{7a}$$

$$m_i^{n\bar{n}}(\rho,\phi) = m_{0i}[2J_1(k_n^{\mathrm{R}}\rho)\sin\phi + 2J_3(k_n^{\mathrm{R}}\rho)\sin 3\phi][I_0(\epsilon k_n^{\mathrm{I}}\rho) - 2I_2(\epsilon k_n^{\mathrm{I}}\rho)\cos 2\phi] \times [J_0(k'_{\bar{n}}\rho) - 2J_2(k'_{\bar{n}}\rho)\cos 2\phi] \tag{7b}$$

$$m_i^{n\bar{n}}(\rho,\phi) = m_{0i}[J_0(k_n^{\mathrm{R}}\rho) + 2J_2(k_n^{\mathrm{R}}\rho)\cos 2\phi][I_0(\epsilon k_n^{\mathrm{I}}\rho) - 2I_2(\epsilon k_n^{\mathrm{I}}\rho)\cos 2\phi] \times [2J_1(k'_{\bar{n}}\rho)\cos\phi - 2J_3(k'_{\bar{n}}\rho)\cos 3\phi] \tag{7c}$$

$$m_i^{n\bar{n}}(\rho,\phi) = m_{0i}[2J_1(k_n^{\mathrm{R}}\rho)\sin\phi + 2J_3(k_n^{\mathrm{R}}\rho)\sin 3\phi][I_0(\epsilon k_n^{\mathrm{I}}\rho) - 2I_2(\epsilon k_n^{\mathrm{I}}\rho)\cos 2\phi] \times [2J_1(k'_{\bar{n}}\rho)\cos\phi - 2J_3(k'_{\bar{n}}\rho)\cos 3\phi] \tag{7d}$$

where the last factors on the second members of (7*a*) and (7*b*) represent the S DE feature, whereas the same factors of (7*c*) and (7*d*) represent the AS DE feature. In (7*a*)–(7*d*) the initial assumption on the complex quantized wavenumber k_n^{C} is given by $k_n^{\mathrm{R}} = k_n^{\mathrm{I}}$. Instead, $k'_{\bar{n}}$ is the corresponding real quantized wavenumber labelling the DE oscillation which is prevalently along the x-direction, but with nodes far from the central region of the dot endfaces and nodal surfaces parallel to the y-direction. The most representative of spin wave modes described by (7*a*)–(7*d*) are those which mix features of EM or AS EM with DE modes. We recall that additional boundary conditions with respect to those obtained by Zivieri and Stamps [6] should be derived for the determination of $k'_{\bar{n}}$.

Let us recall the variational end mode spectrum formulated in [6]:

$$\Omega^2(\tilde{k}_n,\epsilon) = \left[\left(H + E(\tilde{k}_n,\epsilon) - 4\pi M_{\mathrm{s}}\left\langle N_{yy}\left(\rho,\phi=\frac{\pi}{2},\frac{3}{2}\pi\right)\right\rangle_\rho\right) \times \left(H + E(\tilde{k}_n,\epsilon) - 4\pi M_{\mathrm{s}}\left\langle N_{yy}\left(\rho,\phi=\frac{\pi}{2},\frac{3}{2}\pi\right)\right\rangle_\rho + 4\pi M_{\mathrm{s}}[1-\chi(\tilde{k}_n L\sqrt{1+\epsilon^2})]\right)\right] \tag{8}$$

where $E(\tilde{k}_n,\epsilon)$ is the exchange integral. The condition $\frac{\partial\Omega}{\partial\epsilon} = 0$ gives the value of ϵ which minimizes the functional. $\tilde{k}_n = k_n^{\mathrm{R}} \simeq (k_n + k_{n+2})/2$ is the real part of the end mode quantized wavenumber that determines the minimization of the functional. k_n and k_{n+2} are the nth and the $(n+2)$th BA quantized wavenumbers determined by means of the S and AS BA boundary conditions [6] for the specific n which makes possible the functional minimization. For the approximation used to evaluate the averaged static demagnetizing field $H_{\mathrm{s}}^y = -4\pi M_{\mathrm{s}}\langle N_{yy}(\rho,\phi=\frac{\pi}{2},\frac{3}{2}\pi)\rangle_\rho$ of end modes, with $\langle\cdots\rangle_\rho$ labelling the average over the ρ-coordinate see [6].

In this paper we discuss in more detail the restriction used in the variational functional minimization. This restriction is given by the evaluation of the normalization integral given in

equations (55) and (56) of [6] for S and AS end modes, respectively, for an initial value of the variational parameter $\epsilon_{\rm in} = 1$ whereby the minimization is performed. The choice of treating the normalization integral as a constant corresponds to the initial plausible assumption that the real part of the quantized wavenumber is equal to the imaginary part, namely $k_n^{\rm R} = k_n^{\rm I}$. In this way the eigenfunctions of the variational problem are supposed normalized. To demonstrate that this assumption allows us to obtain realistic results we have evaluated the normalization integral for other initial values of ϵ. In this paper the variational procedure has been applied to study the localization of the EM for a dot of Permalloy of radius $R = 100$ nm and thickness $L = 50$ nm (aspect ratio $\beta = 0.5$), but analogous conclusions may also be drawn for other aspect ratios. The material parameters used in all the numerical calculations are those fitted to the BLS data reported in [4] of the continuous Permalloy film: $4\pi M_{\rm s} = 9.5$ kG, $\gamma/2\pi = 2.996$ GHz kOe^{-1}, $\alpha/4\pi = 2.42 \times 10^{-13}$ cm^2. The calculated ρ-averaged demagnetizing tensor component for $\beta = 0.5$ turns out to be $\langle N_{yy}(\rho, \phi = \frac{\pi}{2}, \frac{3}{2}\pi)\rangle_\rho = 0.18$. We have found that the functional may be minimized taking an initial value of $\epsilon_{\rm in}$ in the evaluation of the normalization integral ranging between 0.5 and 1. The minimization has been performed considering an applied field $H = 3$ kOe, because at this field the dot may be considered more uniformly magnetized aside from the region very close to the lateral surface where, due to border effects, the static magnetization is not parallel to the external field. The value of the variational parameter found from the minimization of (8) for an initial $\epsilon_{\rm in} = 0.5$ is $\epsilon \simeq 0.2$ and progressively increases with increasing $\epsilon_{\rm in}$ to become $\epsilon = 0.78$ for $\epsilon_{\rm in} = 1$. Nevertheless, a realistic profile of the EM with important lateral localization is obtained for values of the variational parameter close to $\epsilon = 0.78$. With decreasing ϵ the lateral localization becomes progressively less important and therefore we consider these smaller values of ϵ not to be realistic. Hence, it is plausible to choose $\epsilon_{\rm in} = 1$ as the initial condition for the evaluation of the normalization integral. A similar conclusion may also be drawn for the AS EM. In principle, one could in turn substitute the value of ϵ found from the minimization of (8) into the functional and going on with an iterative procedure looking for a self-consistent minimization. However, even though the functional admits an absolute minimum in the following steps, the corresponding value of ϵ becomes progressively much smaller without reaching convergence and does not give rise to a realistic profile of the EM (AS EM) mode. Hence, we believe that it is plausible to end this minimization procedure at the first step.

Finally, we have also sought an absolute minimum of (8) free from the above limiting assumption, i.e. also taking an ϵ-dependent normalization integral in the minimization, but we have not found an absolute minimum of the variational functional. As a matter of fact, the presence of an absolute minimum strongly depends on the competition between the ϵ-dependent integrals of (8) related to the exchange and to the dipolar fields. Actually, in a physically consistent picture the exchange integral should monotonically increase in modulus with increasing ϵ, because of its square dependence on the quantized wavenumber, whereas the z-component of the dipolar integral should exhibit a monotonically decreasing modulus with increasing ϵ. Assuming an initial ϵ-dependent normalization integral, the exchange integral after an initial increase does have a monotonic decrease with increasing ϵ and the functional cannot be minimized.

We now examine the dependence of the lateral localization on the external field. As pointed out in [6] there is a slight dependence of ϵ on H that does not substantially change the shape of the lateral localization. However, the lateral localization is less important at low fields. The results of this effect are summarized in figure 3 for both the EM and the AS EM at two different values of the applied field. One sees that the lateral localization along the y-direction is less important at $H = 2$ kOe (figures 3(a) and (c)) with respect to the corresponding cases at $H = 3$ kOe for both modes. At $H = 3$ kOe (figures 3(b) and (d)) there are stronger

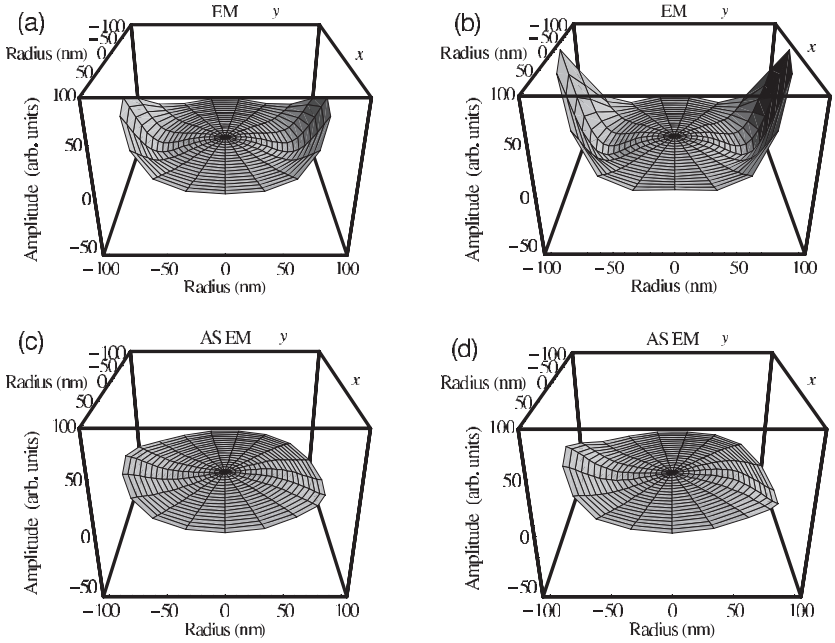

Figure 3. (a) Spatial profile of the EM m_x eigenfunction at $H = 2$ kOe for $\tilde{k}_4 = 6.9 \times 10^5$ cm^{-1}. (b) As in (a), but at $H = 3$ kOe. (c) Spatial profile of the AS EM m_x eigenfunction at $H = 2$ kOe for $\tilde{k}_3 = 5.4 \times 10^5$ cm^{-1}. (d) As in (c), but at $H = 3$ kOe. **H** is applied along the y-axis.

localization effects along the same direction. Indeed, with increasing applied field the value of the variational parameter found from the functional minimization increases corresponding to a larger imaginary part of the quantized wavenumber. The larger ϵ is, the more laterally localized is the mode. In particular, at an external field $H = 2$ kOe we have found that the functional is minimized for $\epsilon = 0.67$ ($\epsilon = 0.58$) for the EM (AS EM); instead, for $H = 3$ kOe the minimization is obtained at $\epsilon = 0.78$ for the EM and at $\epsilon = 0.70$ for the AS EM. The determined quantized wavenumbers are $\tilde{k}_4 = 6.9 \times 10^5$ cm^{-1} for the EM and $\tilde{k}_3 = 5.4 \times 10^5$ cm^{-1} for the AS EM. The assigned value is substantially independent of the dot thickness and is obtained from the boundary condition of the S BA and AS BA modes given in equations (44) and (45), respectively of [6] from which k_4 and k_6 for EM and k_3 and k_5 for AS EM are determined. We recall that for the dot studied ($R = 100$ nm and $L = 50$ nm) the internal field is larger than zero for an applied magnetic field larger than about 1 kOe and that the variational functional (8) admits a minimum for a larger applied magnetic field, i.e. for $H > 1.7$ kOe. Moreover, when the minimization is performed for 1.7 kOe $< H < 3$ kOe lower values of ϵ are found yielding to lower frequencies with respect to those obtained for $H = 3$ kOe. Again, we stress that the minimization performed at a high external field ($H = 3$ kOe) is more realistic. The ϵ found at this field has thus been assumed to be valid for the frequency calculation in the whole range of H corresponding to the saturated state, i.e. for 1 kOe $< H < 3$ kOe.

Note that also for $\tilde{k}_n$ with $n > 4$ for S end modes ($n > 3$ for AS end modes) absolute minima are found for $H = 3$ kOe and for lower applied fields ranging more or less in the same interval as those examined for the EM and the AS EM. These larger $\tilde{k}_n$ would correspond to the second S end mode (AS end mode) of the family. Also these modes have a lateral localization

without nodes throughout the dot. Indeed, as remarked by Bayer *et al* for thin stripes [13] and as already pointed out in [6] for cylindrical dots, with increasing applied field the internal field, which may be represented as a potential barrier in the central part of the dot endfaces, increases creating multiple localized states in the lateral part. It is worth noting that the shape of the lateral localization along the direction of the static magnetization of the single localized mode is not substantially affected by the increase of the magnitude of the applied field showing a very similar behaviour to that shown by the EM and the AS EM profiles, except for the presence of slight localization effects also along the x-direction. However, we do not give here the profiles of these modes, because they do not allow us to draw further interesting conclusions about lateral localization.

Let us now discuss in more detail the two ϵ-dependent integrals, i.e. the exchange integral and the dipolar integral. Although the quantized wavenumber of the end modes is assumed complex it is important to note that both integrals are real. In particular, the exchange integral could in turn be complex too, but it turns out to be real because of the assumed real eigenfunctions of end modes given in (5) and (6). As outlined in [6], since these modes are localized close to the dot edges it seems realistic to consider their exchange contribution evaluating the exchange integral on the dot border, i.e. for $\rho = R$, even though this approximation could give rise to a slight source of error in the frequency calculation. In particular, for the dot studied the numerical value of the EM exchange integral that corresponds to the dynamic exchange field turns out to be $E^4(\tilde{k}_4 = 6.9 \times 10^5\ \mathrm{cm}^{-1}, \epsilon = 0.78) \simeq 500$ Oe. The corresponding AS EM exchange integral is slightly larger, i.e. $E^3(\tilde{k}_3 = 5.4 \times 10^5\ \mathrm{cm}^{-1}$, $\epsilon = 0.70) \simeq 600$ Oe. The dependence on the i index ($i = x, z$) is omitted, because within this model the exchange integral corresponding to the x and z dynamic magnetization components is the same. Note that at this stage also the normalization integrals N^3 and N^4 appearing in the expressions for E^3 and E^4 are evaluated for $\epsilon = 0.70$ and $\epsilon = 0.78$, respectively, found from the functional minimization. In both cases the corresponding dynamic exchange field gives a non-vanishing contribution to the effective field.

On the other hand, the dynamic dipolar integral is also real in spite of the complex quantized wavenumber. As a matter of fact, the z-component of the dynamic dipolar field $h_{\mathrm{d}}^z(\boldsymbol{\rho}) \simeq -4\pi[1 - \chi(\tilde{k}L\sqrt{1+\epsilon^2})]m_z(\boldsymbol{\rho})$ has been obtained within the thin film approximation that is assumed valid for dots of small aspect ratio. Within this approximation the real wavevector of the momentum representation of the Green's function appearing in the expression of the dipolar field is quantized and is treated on the same footing as the mode quantized wavenumber which is taken in modulus. We remind that, with increasing aspect ratio, this approximation becomes progressively less valid. For the dot studied ($R = 100$ nm, $L = 50$ nm) the z-component of the EM dynamic dipolar integral for $\epsilon = 0.78$ and for $\tilde{k}_4 = 6.9 \times 10^5\ \mathrm{cm}^{-1}$ turns out to be in modulus $|d_z^4| \simeq 2150$ Oe. The corresponding AS EM calculated value for $\epsilon = 0.70$ and $\tilde{k}_3 = 5.4 \times 10^5\ \mathrm{cm}^{-1}$ is $|d_z^3| \simeq 2800$ Oe. For both modes the dipolar field contributes significantly to the effective field.

5. Comparison with experimental data

In this section we compare the calculated frequencies of some of the localized modes discussed in the previous sections with the experimental data. As demonstrated from scattering cross section calculations [5] S modes with no nodes or with a low number of nodes throughout the dot give a non-vanishing contribution to the cross section. This is the case of the F mode that has the largest cross section in the spectrum and of the EM whose cross section is also appreciable.

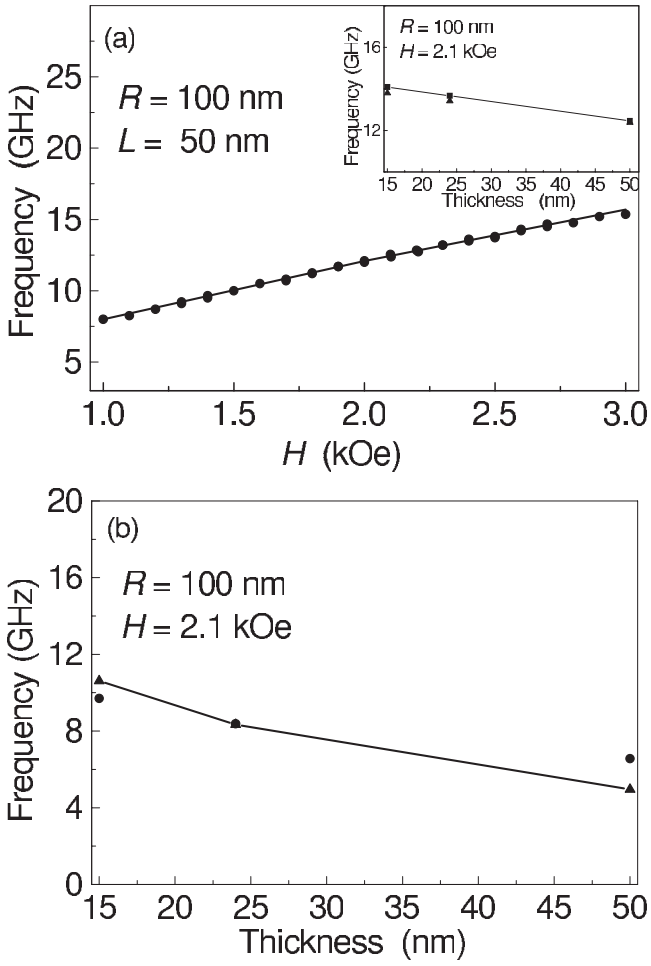

Figure 4. (a) F mode dispersion versus the applied field. Circles: BLS data from [4]. Continuous line: calculated frequency. Inset: F mode dispersion versus thickness for $R = 100$ nm at $H = 2.1$ kOe. Up triangles: BLS data at $L = 15$ and $L = 24$ nm from [6] and at $L = 50$ nm from [4]. Squares: calculated frequencies. The line connecting the symbols is a guide to the eyes. (b) Frequency dispersion of the EM versus thickness. Circles: BLS data at $L = 15$ and 24 nm from [6] and at $L = 50$ nm from [4]. Up triangles: calculated frequencies. The line connecting the symbols is a guide to the eyes.

In figure 4(a) the frequency of the F mode determined according to (4) is calculated for a dot of Permalloy of radius $R = 100$ nm and thickness $L = 50$ nm and is compared with the BLS frequency as a function of the applied magnetic field. The calculated frequency excellently agrees with the measured one for the whole range of H. The F mode dispersion as a function of thickness for $R = 100$ nm and at the external field $H = 2.1$ kOe is shown in the inset to figure 4(a). One notes that the frequency decreases with increasing dot thickness. Also in this case the agreement between theoretical calculations and measurements is very good. In figure 4(b) the EM dispersion as a function of the dot thickness calculated for a dot of radius $R = 100$ nm and for three thicknesses $L = 15$ nm, $L = 24$ nm and $L = 50$ nm, respectively, is compared with BLS frequencies for an external field $H = 2.1$ kOe. As shown,

the overall agreement is good. As already pointed out in [6] the slight discrepancy between the calculated and the experimental frequency at $L = 15$ nm could be due to the overestimation of the exchange integral that is evaluated solely from its contribution on the border and is not calculated throughout the whole dot. As shown in [6] this discrepancy becomes larger for higher applied fields. Nevertheless, for $L = 24$ nm where the calculated frequency excellently agrees with the experimental one it seems that this source of error is no longer present. It is important to note that the assumptions made in the minimization of the functional, like for example the initial choice of the normalization integral treated as a constant, the assignment of the quantized wavenumber $\tilde{k}_n$ of the end modes determined from the boundary condition of the BA modes and the search for an absolute minimum made at a fixed external field $H = 3$ kOe could be sources of error in the determination of the EM frequency. Finally, the diagonal approximation used to calculate the eigenfrequencies could also add a further small error in the determination of the EM frequency. From figure 4(b) one also sees that the calculated EM frequency at $L = 50$ nm underestimates the experimental frequency. This disagreement is not present only for $H = 2.1$ kOe, but also for other applied fields not reported here; hence, it may be considered as a general disagreement. In addition to the previous probable reasons for discrepancy it is possible that for this moderate aspect ratio ($\beta = 0.5$), and also for the determination of the EM frequency, the thin film approximation made for the calculation of the dipolar contribution together with the assumption of a uniform dynamic magnetization profile across the thickness of the dot could be less realistic. We expect that, as stated for the case of BA modes studied in [6], the exact calculation of the dipolar contribution together with the introduction of a z-dependence for the dynamic magnetization should upshift the EM frequency at $L = 50$ nm towards the experimental value.

6. Conclusions

In this paper the variational method recently formulated to describe the dynamical properties of spin modes in tangentially magnetized thin cylindrical dots has been applied to study the most representative excitations of the spectrum. The analysis has been performed for dots of size in the nanometric range with a fixed radius and for different aspect ratios. The frequency of the F mode, the most representative of the spectrum, has been found according to an approximated formula derived by means of the Kittel equation of ellipsoids written for cylindrical dots. This approximated formula has been applied to a dot of moderate aspect ratio ($\beta = 0.5$), but is also valid for dots of smaller aspect ratios. A comparison with BLS experimental frequency has been performed by studying both the dependence of the external magnetic field at a fixed aspect ratio and the dependence of the dot thickness at a fixed radius and for a specific external magnetic field. The general agreement between calculations and experimental data is very good.

Moreover, the dynamical properties of the most representative end modes have been investigated. The main restriction of the variational method has been discussed assuming different initial choices of the normalization integral and showing that the most appropriate is the one corresponding to the initial choice that the real part of the quantized wavenumber is equal to the imaginary part. The overall agreement of the calculated frequency of the EM as a function of the dot thickness with the measured one is good for low aspect ratios ($\beta < 0.25$), but is less convincing for moderate aspect ratios (for example for $\beta = 0.5$). Trial eigenfunctions of spin modes which mix end mode features with DE features have also been proposed.

Furthermore, the local approximation based on the thin film assumption, which also includes our neglect of the z-dependence in the profile of the dynamic magnetization across the dot thickness, seems less realistic in dots of moderate aspect ratio and for the case of

end modes. Finally, in order to further generalize the theory, a variational expression for the dynamic nonuniform exchange field of the end modes without any initial limiting assumption should be found to minimize the frequency functional.

Acknowledgments

We would like to thank F Nizzoli for very useful discussions. Financial support by Ministero Università e Ricerca (grant PRIN 2004027288) is acknowledged.

References

[1] Jorzick J, Demokritov S O, Hillebrands B, Bartenlian B, Chappert C, Decanini D, Rousseaux F and Cambril E 1999 *Appl. Phys. Lett.* **75** 3859
[2] Demokritov S and Hillebrands B 2002 *Spin Dynamics in Confined Magnetic Structures I* (*Springer Series in Topics in Applied Physics*) ed B Hillebrands and K Ounadjela (Berlin: Springer)
[3] Guslienko K Yu and Slavin A N 2000 *J. Appl. Phys.* **87** 6337
[4] Gubbiotti G, Carlotti G, Okuno T, Shinjo T, Nizzoli F and Zivieri R 2003 *Phys. Rev.* B **68** 184409
[5] Giovannini L, Montoncello F, Nizzoli F, Gubbiotti G, Carlotti G, Okuno T, Shinjo T and Grimsditch M 2004 *Phys. Rev.* B **70** 172404
[6] Zivieri R and Stamps R L 2006 *Phys. Rev.* B **73** 144422
[7] Joseph R I and Schlömann E 1965 *J. Appl. Phys.* **36** 1579
[8] Kittel C 1948 *Phys. Rev.* **73** 155
[9] Brown W F Jr and Morrish A H 1958 *Phys. Rev.* **105** 1198
[10] Zivieri R and Nizzoli F 2005 *Phys. Rev.* B **71** 014411
Zivieri R and Nizzoli F 2006 *Phys. Rev.* B **75** 1 (erratum)
[11] Jorzick J, Demokritov S O, Hillebrands B, Bailleul M, Fermon C, Guslienko K Y, Slavin A N, Berkov D V and Gorn N L 2002 *Phys. Rev. Lett.* **88** 047204
[12] Gubbiotti G, Carlotti G, Okuno T, Grimsditch M, Giovannini L, Montoncello F and Nizzoli F 2005 *Phys. Rev.* B **72** 184419
[13] Bayer C, Demokritov S O, Hillebrands B and Slavin A N 2003 *Appl. Phys. Lett.* **82** 607